

VARIATIONS OF SOME SPECTRAL LINES IN THE SPECTRUM OF V 1295 AQL

G. R. Bahaddinova^{a,b}, *N. Z. Ismailov*^a, *U. Z. Bashirova*^{a*}

^a *N. Tusi Shamakhy Astrophysical Observatory of Azerbaijan National Academy of Sciences, Shamakhy, Azerbaijan*

^b *Khazar University, Baku, Azerbaijan*

The results of homogeneous spectral observations of the HAeBe-type star V1295 Aql obtained in 2016–2020 are presented. The variability of the profiles of the $H\alpha$, $H\beta$, FeII, SiII, [OI], D NaI spectral lines is considered. The Fe II lines show two emission peaks with central absorption, with the variable displacement from +15 to -5 km/s in different years. Almost all metal lines show changes in the radial velocity and the equivalent width of the emission components. The profile structure show variability in a complex form, but more often with two peaks superimposed on the line wings. The same structures in profiles also observed in purely absorption lines. [OI] $\lambda 6300$ Å line shows a weak form redshift, indicating the observation of accretion in the outer layers. Despite this, most likely, the star has a strong chromosphere activity.

Keywords: pre-main sequence stars – spectral variations – circumstellar matter – emission lines – Ae stars, individual: V1295 Aql.

1. INTRODUCTION

HAeBe stars [1] defined the massive counterparts of T Tauri stars (TTs) as emission line objects with spectral type A or earlier that locate in obscured regions and illuminate bright and close nebulosities. Currently, Herbig Ae/Be stars (HAeBe) are known as young ($\lesssim 10$ Myr), optically visible pre-mainsequence (PMS) stars with emission lines in their spectra, typical spectral types A and B, stellar masses that typically range between ~ 2 and $\sim 12M_{\odot}$, and infrared (IR) excesses associated with circumstellar disks. The spectroscopic monitoring of some sources [2–4] revealed that the spectra of HAeBe objects are not only characterized by the presence of emission lines, but also by the complex varia-

* E-mail: gunelbahaddinova@gmail.com

tions observed in both the emission and absorption features. This variability is also characteristic of T-Tauri stars [5, 6].

V1295 Agl (HD190073, MWC325, A2IIIe - B9IIep+sh) is a very remarkable early-type object with rich emission lines in the visible spectrum. HD190073 was variously classified as a peculiar Bep star [7] or as an evolved post-main sequence A giant [8]. Recently HD190073 has gained recognition as a young Herbig Ae/Be star [9, 10]. Despite being situated in the constellation of Aquila far from wellknown regions of star formation, it displays a large far-IR excess due to thermal radiation of cool circumstellar (CS) dust [11]. The energy distribution of HD190073 in this spectral region is similar to that of well-known Herbig Ae stars, like AB Aur, HD163296 and HD31648 [12].

Alicia et al. [13] identified stellar parameters for V1295 Agl. The star has a magnetic field, $\sim 100\text{G}$, which has been detected and confirmed by many authors over several years [14–16]. As described in [13] from MIKE spectra $V_r = -1.2 \pm 1.3 \text{ km/s}$ and $v \sin i = 3.19 \pm 2.45 \text{ km/s}$. Effective temperature is $T_{\text{eff}} = 9250 \pm 250 \text{ K}$, Mass is $M_* = 2.9 \pm 0.5 M_{\odot}$ radius is $R_* = 3.6 \pm 0.5 R_{\odot}$. Variability was observed, indicating a change in the star’s magnetic field structure.

In this work, we have presented new results of monitoring of the spectral lines $H\alpha$, $H\beta$, FeII, SiII, [OI], D NaI on the spectral observations of the star in 2016-2020.

2. OBSERVATIONS

The spectra were carried out in the 2-m telescope of Shamakhy Astrophysical Observatory of Azerbaijan National Academy of Sciences. We used ShAFES spectrographs that works with CCD $4 \text{ K} \times 4 \text{ K}$, spectral resolution is $R \sim 28000$ in wavelength range $\lambda 3700 - 8000$ [17]. The mean signal-tonoise level is $S/N \sim 100$ in the region of the H_{α} line, and $S/N = 40 - 60$ in the region of the H_{β} line. Wavelength calibration have made on the sky and ThAr lamp spectrum. For calibration and processing of spectrograms used the DECH20T software [18]. We used total of 27 pairs of spectrograms of the star for 2016-2022 years. The mean error of positional measurements in the spectra of standard stars was $0.5 - 1 \text{ km/s}$, and standard deviations in intensities at 0.5% .

3. MAIN RESULTS

Results for the $H\alpha$ line

In this work, we have created average profiles and standard deviation its intensity along the wavelength for the lines H_{β} , Fe II, Si II, [O I], D Na I, for 2016-2020

years. We monitored their variation for each year. In the Fig.1 is presented average profile (solid line) and standard deviation σ of the line intensity for each point along wavelength (dashed line) of H_{α} line. As it is seen from Fig.1 H_{α} line is emission line. In 2016 and 2017 years it has got barely distinguished two picks. But in 2018-2022 years it shows only red component. In 2016 and 2018 years standard deviation shows some variations. In 2016 year, it shows variation in red component, but in 2018 in blue component. In the Table 1 is shown radial velocities of H_{α} line's red, blue component and full wide (FW) at the 10% intensity level and radial velocity of standard deviation in 10% intensity level. Last two rows show average value of radial velocity and standard deviation. As it is seen from Table 1 , the full wide of the line at 10% level of intensity is not more than 300 km/s. It means that there is no strong accretion and wind features.

Table 1. Profile parameters of the H_{α} line's red, blue component and full wide in 10% intensity level and radial velocity of standard deviation in 10% intensity level.

Year	RV_b (km/s)	RV_r (km/s)	FWat 10% (km/s)	σ_b (km/s)	σ (FW) 10% (km/s)	σ_r (km/s)
2016	16.5	52.5	-223	241	-273	231
2017	4.5	7.5	-269	201	-291	121
2018		44	-194	241	-200	187
2019		49.5	-171	214	-174	176
2020		45	-153	220	-207	200
Average	10.5	39.7	-202	223.4	-229	183
rms	8.5	18.3	45.7	17.5	50.3	40.3

The $H\beta$ line

$H\beta$ line is an absorption line with central emission component. Absorption wings are typical photospheric wings. In the Fig. 2, as in Fig.1 is presented average profile and its standard deviation of the $H\beta$ line. From standard deviation of profile, we carried out that there is no obvious change in the wings of line, but we can observe variation in the emission component mainly in 2016 and 2018 year. This variation is synchronous with the variation in profile of the H_{α} line in 2016 and 2018 years.

In the Table 2 is shown radial velocities of $H\beta$ line's red and blue component and FW in 10% intensity level and FW of standard deviation in 10% intensity

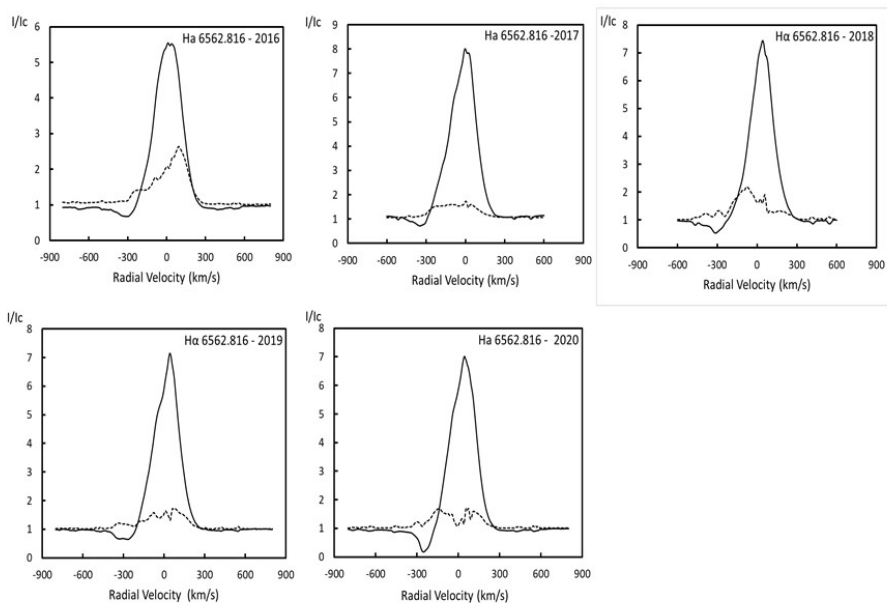


Fig. 1. H_{α} profiles (solid lines) and standard deviation of intensity along the wavelength (dashed lines) for 2016-2020 years.

level. Last two rows show average value of radial velocity and standard deviation.

Table 2. Radial velocity of $H\beta$ line's red, blue component and in 10% intensity level and radial velocity of standard deviation in 10% intensity level.

Year	RV_b (km/s)	RV_r (km/s)	FW10% (km/s)	σ_b (km/s)	σ FW 10% (km/s)	σ_r (km/s)
2016	-76	54.5	-109	103	-219	191
2017	-86	16.5	-173	138	-286	129
2018	-59	50.5	-77	121	-212	8.5
2019	-49	29	-150	89.5	-277	117
2020	-36	60	-110	121	-269	164
Average	-61.2	42.1	-123.8	114.5	-252.6	121.9
rms	20.1	18.5	37.8	18.7	34.5	69.8

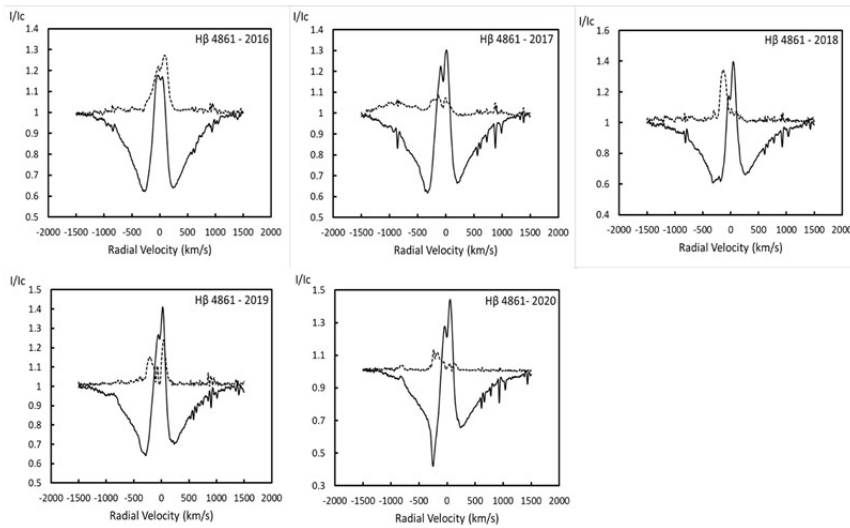


Fig. 2. H_{β} profiles (solid lines) and standard deviation of intensity along the wavelength (dashed lines) for 2016-2020 years.

The line Fe II 4924

FeII $\lambda 4924 \text{ \AA}$ emission line shows 2 emission peaks with central absorption. In the Fig.3 is presented average profile and standard deviation of FeII $\lambda 4924 \text{ \AA}$ line for each year. Standard deviation varies in 2016 and 2019 years. Variation in 2019 is not synchronous with $H\alpha$ line.

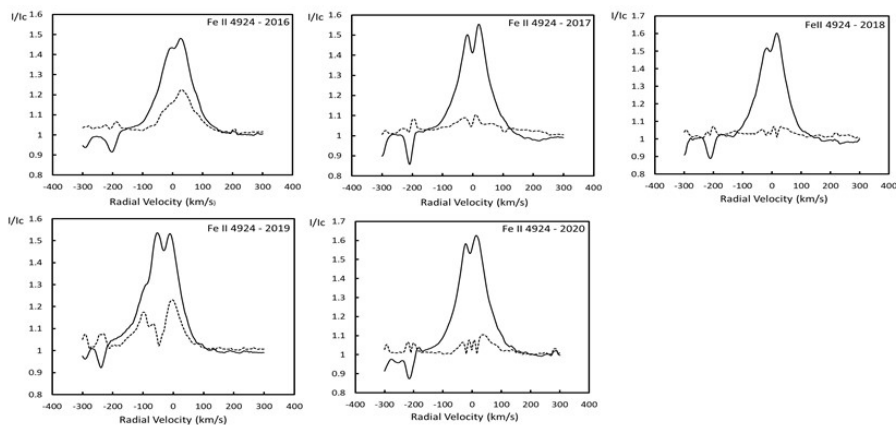
In the Table 3 is shown radial velocities of the FeII $\lambda 4924 \text{ \AA}$ line's red and blue components and FW in 10% of intensity level and its standard deviation parameter FW10%. Last two rows show average value of radial velocity and standard deviation σ .

The line FeII $\lambda 5018 \text{ \AA}$

The FeII $\lambda 5018 \text{ \AA}$ is also emission line with central absorption. Standard deviation of the line profile exhibit some variability in 2019. The character of variations in the FeII lines is similar, but significantly different with the activity dates with of the $H\alpha$ line profiles. It is indicated that variability in profiles of the FeII lines may be results of chromospheric activity. The standard deviation in other years is close to the noise level, which indicates the absence of significant variations in the profile. In the Table 4 is presented radial velocities the of FeII $\lambda 5018 \text{ \AA}$ line's red and blue components and parameter FW10% and its standard

Table 3. Radial velocity of FeII $\lambda 4924 \text{ \AA}$ line's red and blue components, FW10% parameter and its standard deviation and its FW10% parameter.

Year	RV_b (km/s)	RV_r (km/s)	FW10% (km/s)	σ_b (km/s)	σ FW 10% (km/s)	σ_r (km/s)
2016	-1.43	24	-112	135	-53	123
2017	-20	24	-106	117	-62	69
2018	-22	21	-105	97	-38	44
2019	-52.2	-8	-147	56	-128	54
2020	-22	10.5	-124	119	-42	78
Average	-23.526	14.3	-118.8	104.8	-64.6	73.6
Standard deviation	18.2	13.6	17.5	30.4	36.7	30.6

**Fig. 3.** Average profiles (solid line) and standard deviation (dashed lines) of Fe II $\lambda 4924 \text{ \AA}$ line for 2016-2020 years.

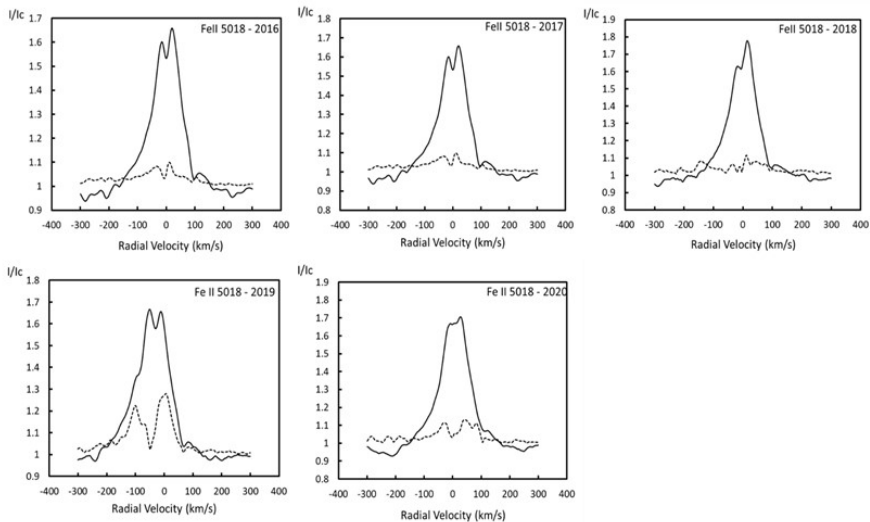
deviation. Last two rows show average value of radial velocity and its standard deviation.

The line FeII $\lambda 5169$

In the Fig. 5 is shown the average profiles of the FeII $\lambda 5169 \text{ \AA}$ line for 2016-2020 years. This line shows two emission components in 2017, 2018, 2020 years but one peak in 2016 and 2019 years. Standard deviation of profile exhibit some variations in 2016 and 2019 years. Variation in 2016 year observed in all line's of

Table 4. Profile parameters of the FeII λ 5018 Å line's red and blue components and FW10%.

Year	RVb (km/s)	RVr (km/s)	FW 10% (km/s)	σ_r (km/s)
2016	1	22	-108	99.5
2017	-18.5	18	-132	88
2018	14.5	12	-110	81.5
2019	-47.5	-8	-158	53
2020	-11.5	23	-133.5	138
Average	-12.4	13.4	-128.3	92
rms	23.3	12.7	20.4	30.9

**Fig. 4.** Average profiles (solid lines) and standard deviation (dashed lines) of the Fe II λ 5018 Å line for 2016-2020 years.

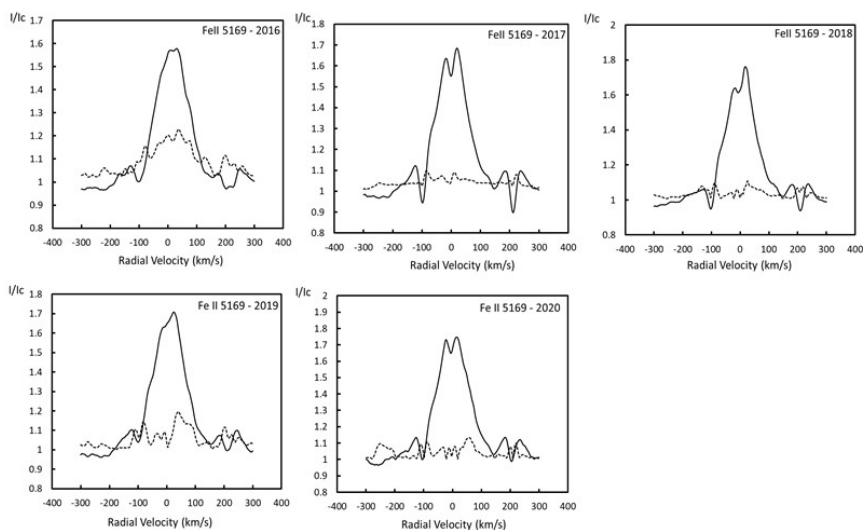
the average profiles. In the Table 5 it is presented profile parameters of the line FeII λ 5169 Å line's red and blue components and parameter FW10%.

The line Fe I λ 4958 Å

As it seen from Fig. 6. Fe I λ 4958 Å is an absorption line. This line is pure photospheric line. Standard deviation of this line shows two picks, so it shown that the line structure changes in its red and blue wings. Rather than we see in the wings some variability due to the star exhibited photospheric activity in this

Table 5. Profile parameters of the Fe II λ 5169 Å line's red and blue components and FW10%..

Year	RV_b (km/s)	RV_r (km/s)	FW 10% (km/s)	σ_r (km/s)
2016	15	28.5	-79	122
2017	-15.5	22.5	-83.5	106
2018	-16.5	20.5	-78.5	118
2019	-11	28.5	-74.5	118
2020	-18.5	18	-90	127
Average	-9.3	23.6	-81.1	118.2
Standard deviation	13.9	4.7	5.9	7.8

**Fig. 5.** Average profiles (solid lines) and standard deviation (dashed lines) of the Fe II λ 5169 Å line for 2016-2020 years.

line. Variability dominated mainly in the red wing in all years. In the Table 6 is presented the same profile parameters for the line Fe I λ 4958 Å.

The Si II λ .6371 Å & line

In the Fig. 7 is shown the average profile of Si II λ 6371 Å absorption line for each year. It is also absorption line, and its profiles are same to the profiles of

Table 6. Profile parameters of the line Fe I $\lambda 4958 \text{ \AA}$ and its standard deviation parameters.

Year	RV_a (km/s)	RV_b (km/s)	RV_r (km/s)	FW10% (km/s)	σb (km/s)	σ FW10% (km/s)	σ_r (km/s)
2016	-5	-14	16	-60	36	-53	40
2017	0	-14	16	-33	21	-31	33
2018	-6	-26	4	-34	14	-35	20
2019	-3	-27	6.5	-48	19.5	-52	48.5
2020	-11.5	-30.5	6	-34	12	-35.5	20.5
Average	-5.1	-22.3	9.7	-41.8	20.5	-41.3	32.4
rms	4.2	7.8	5.8	11.9	9.4	10.4	12.4

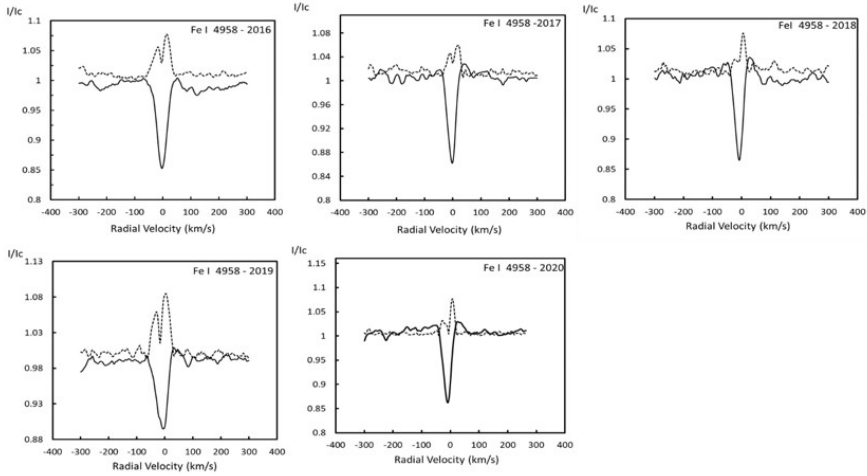


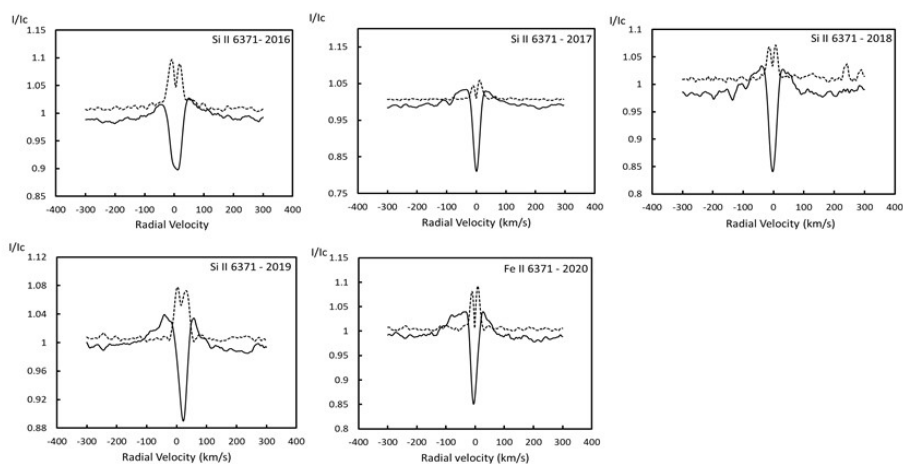
Fig. 6. Average profiles (solid lines) and standard deviation (dashed lines) of the Fe I $\lambda 4958 \text{ \AA}$ line for 2016-2020 years.

the Fe I $\lambda 4958 \text{ \AA}$ line. In all years, in average profile we can see main absorption component, which has weak emission components superimposed to wings. Standard deviation of the profile also exhibit two picks that shows variation in blue and red wings.

Table 7. shows radial velocities of Si II 6371 line’s absorption component and in 10% intensity level and radial velocity of standard deviation in 10% intensity level and in picks. Last two rows show average value of radial velocity and standard deviation.

Table 7. Profile parameters of the line Si II $\lambda 6371 \text{ \AA}$ and its standard deviation parameters.

Year	RV_a (km/s)	RV_b (km/s)	RV_r (km/s)	FW10% (km/s)	σ_b (km/s)	σ FW10% (km/s)	σ_r (km/s)
2016	13.5	-7	21	-26	34	-32	35
2017	2	-7	13.5	-19	21	-24	41
2018	-1.5	-11.5	9	-24.5	20.5	-28.5	19
2019	24	5.5	33.5	-18.5	54.5	-19	51
2020	-5	-11	11.5	-21.5	28.5	-22.5	23
Average	6.6	-6.2	17.7	-21.9	31.7	-25.2	33.8
rms	11.9	6.9	9.9	3.3	13.9	5.1	13.1

**Fig. 7.** Average profiles (solid lines) and standard deviation (dashed lines) of the Si II $\lambda 6371 \text{ \AA}$ line for 2016-2020 years.

The D1, D2 Na I lines

Both of sodium lines exhibit two strong emission peaks with the dib central absorption. In the Fig. 8 and Fig.9 is presents average profiles of the D1, D2 Na I line. Radial velocities of the central absorption peak shows stability, because we suggested that the central absorption component is formed in the photosphere. As it is seen from profiles, there are variation in all years mainly in blue and more intensive red component.

In the Table 8 and Table 9 it is presented radial velocities of both doublet lines red and blue components and FW in 10% intensity level. Last two rows show average value of radial velocity and standard deviation (rms).

Table 8. Radial velocities of D2 Na I line's red and blue component and in 10% intensity level line.

Year	RV_b (km/s)	RV_r (km/s)	FW10% (km/s)	σ FW (km/s)
2016	-34.5	41	-91	86.5
2017	-30.5	27	-91.5	77
2018	-38	41.5	-95	82
2019	-35	28.5	-63.5	64
2020	-39.5	27	-102	75.5
Average	-35.5	33	-88.6	77
rms	3.5	7.5	14.7	8.5

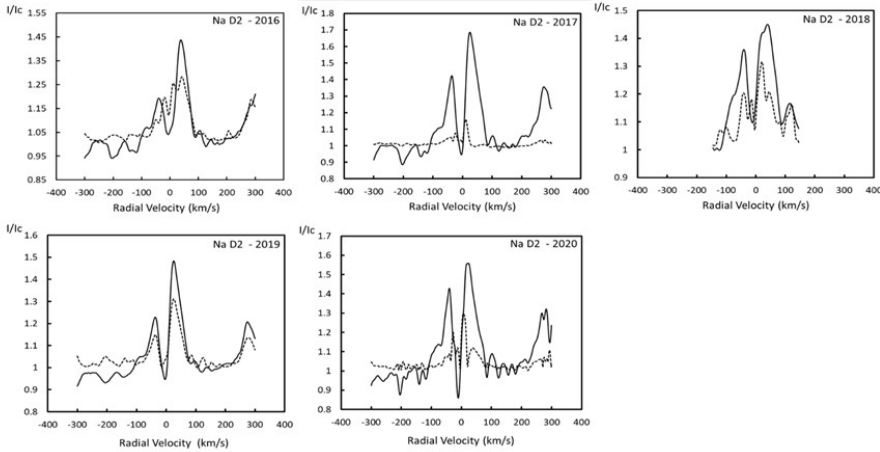


Fig. 8. Average profiles (solid lines) and standard deviation (dashed lines) of the D2 Na I line for 2016-2020 years.

Profile and structure of Na D1 line's standard deviation is similar with D2 Na I line (Fig.9). In 2016 it shows only one emission component but in other years two emission picks with central absorption is observed.

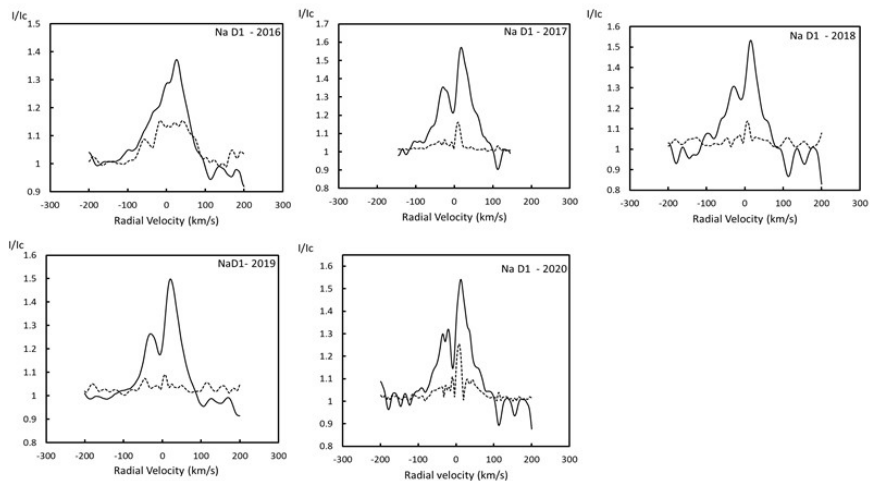


Fig. 9. Average profiles (solid lines) and standard deviation (dashed lines) of the D2 Na I line for 2016-2020 years.

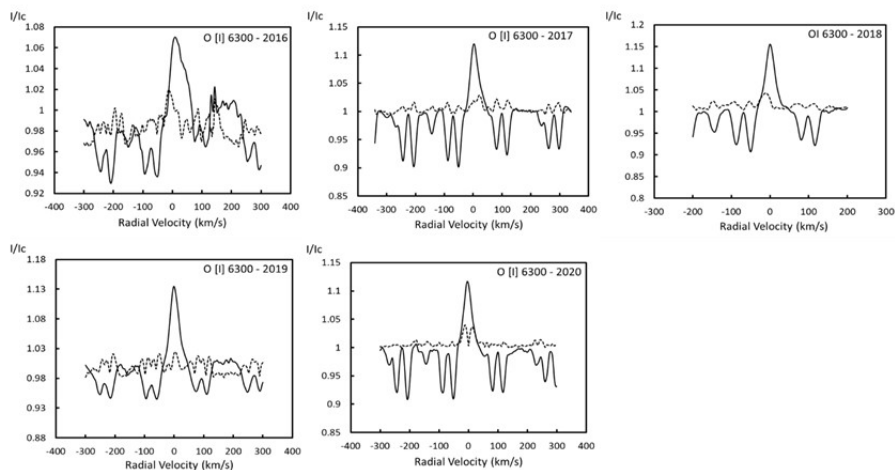


Fig. 10. Average profiles (solid lines) and standard deviation (dashed lines) of the [OI] λ 6300 Å line for 2016-2020 years.

The [OI] λ 6300 Å line

As seen from figure10 [OI] λ 6300 Å the line is in emission and show little variations in radial velocities. Standard deviation of average profiles mainly is stable, except of weak form variability in data of 2016 and 2020.

Table 9. Radial velocities of D1 Na I line's red and blue component and FW in 10% intensity level line.

Year	RV_b (km/s)	RV_r (km/s)	FW10% (km/s)	σ FW (km/s)
2016	5.5	26.5	-62.5	80
2017	-25.5	20.5	-73	81.5
2018	-19	17	-73.5	69
2019	-28	23.5	-55	65
2020	-21	13.5	67.8	73
Average	-17.6	20.2	-39.24	73.7
Standard deviation	13.4	5.1	60.3	7.0

Table 10 shows radial velocities of [OI] $\lambda 6300$ Å lines in pick and FW in 10% of intensity level and its standard deviation.

Table 10. Radial velocities of [OI] $\lambda 6300$ Å line's in pick and FW in 10% intensity level.

Year	RV (km/s)	FW 10% (km/s)	σ FW (km/s)
2016	13.5	-18.5	65.5
2017	6.5	-21	50
2018	2	-30	29.5
2019	-0.5	-22.5	24.5
2020	-1.5	-27.5	37
Average	4	-23.9	41.3
rms	6.1	4.7	16.6

4. CONCLUSIONS

The average profile and structure of the $H\alpha$ line show strong variability in 2016 and 2018 years but in other years variability of the profiles is weak. Significant accretion and wind features are not observed, since the full wide of the line at the 10% intensity level are less than 300 km/s.

Variability in $H\beta$ and $H\alpha$ lines are similar, but obviously observed blue and red components in the $H\beta$. As well for emission component width of the $H\beta$ line is thinner than the width of $H\alpha$.

The activity observed in the metal lines does not coincide with the cycle of activity in the hydrogen lines in different seasons. It also shows that the reason for the activity in metal lines can be related to chromosphere activity (magnetic spots on the surface, flares). A variation with a two-peaked structure was found in both the red and blue wings of each metal lines with an absorption profile and with visible emission component in their wings. This indicates possible frequent flares in the star's photosphere. of the star. The strong variation has not observed in this line. Only weak accretion is defined from the outer layers.

REFERENCES

1. Herbig G.H., 1960, Ap.J. Suppl.Ser., **4**, 337
2. Praderie F., Simon T., Catala C., & Boesgaard A.M., 1986, Ap.J. Letters, **303**, 3
3. Pogodin M. A., 1994, Astron.& Astrophys., **282**, 14
4. Rodgers B., Wooden D.H., Grinin V., et al., 2002, AJ, **564**, 405
5. Johns C. M., & Basri G., 1995, AJ , **109**, 2800
6. Schisano E., Covino E., Alcalá J.M., et al., 2009, Astron.& Astrophys., **501**, 1013
7. Allen D. A., & Swings J. P., 1976, Astron. & Astrophys., **47**, 293
8. Cuttela M., & Ringuelet A. E., 1990, MNRAS, **246**, 20
9. Cidale L., Zorec J., & Morrell N., 2000, The Be Phenomenon in Early-Type Stars, ASP Conf. Ser., in IAU Colloq.175, **214**, 87
10. de Winter D., van den Ancker M. E., Maira A., et al., 2001, Astron.& Astrophys., **380**, 609
11. Sitko M. L., 1981, ApJ., Letters, **247**, 1024
12. Malfait K., Bogaert E., & Waelkens C., 1998, Astron.&Astrophys., **331**, 211
13. Alicia N. Aarnio , John D. Monnier ., et al., 2017, ApJ Letters, **18**, 34
14. Hubrig S., Yudin R.V., Schöller M., Pogodin M.A., 2006, Astron.&Astrophys., **446**, 1089
15. Hubrig S., Stelzer B., Schöller M., et al., 2009, Astron.&Astrophys., **502**, 283
16. Catala C., Alecian E., Donati J. F., et al., 2007, Astron.&Astrophys., **462**, 293
17. Mikayilov Kh.M., Musayev F.A., et al., 2017, AzAJ, **12(1)**, 4.
18. Galazutdinov G. <http://www.gazinur.com/DECH-software.html>.